Published in final edited form as:
J Med Chem. 2009 October 8; 52(19): 6073–6082. doi:10.1021/jm900940f.

Synthesis and small-animal positron emission tomography evaluation of [^{11}C]-elacridar as a radiotracer to assess the distribution of P-glycoprotein at the blood-brain barrier

Bernd Dörner[a], **Claudia Kuntner**[b], **Jens P. Bankstahl**[c], **Marion Bankstahl**[c], **Johann Stanek**[d], **Thomas Wanek**[b], **Gloria Stundner**[b], **Severin Mairinger**[a,b,d], **Wolfgang Löscher**[c], **Markus Müller**[d], **Oliver Langer**[b,d,*], and **Thomas Erker**[a]

[a]Department of Medicinal Chemistry, University of Vienna, Austria

[b]Molecular Medicine, AIT Austrian Institute of Technology GmbH, Seibersdorf, Austria

[c]Department of Pharmacology, Toxicology & Pharmacy, University of Veterinary Medicine Hanover, Germany

[d]Department of Clinical Pharmacology, Medical University of Vienna, Austria

Abstract

With the aim to develop a positron emission tomography (PET) tracer to assess the distribution of P-glycoprotein (P-gp) at the blood-brain barrier (BBB) *in vivo*, the potent third-generation P-gp inhibitor elacridar (**1**) was labeled with ^{11}C by reaction of *O*-desmethyl **1** with [^{11}C]-methyl triflate. *In vitro* autoradiography and small-animal PET imaging of [^{11}C]-**1** was performed in rats (n=3), before and after administration of unlabeled **1**, as well as in wild-type, *Mdr1a/b*$^{(-/-)}$ and *Bcrp1*$^{(-/-)}$ mice (n=3). In PET experiments in rats, administration of unlabeled **1** increased brain activity uptake 5.4-fold, whereas blood activity levels remained unchanged. In *Mdr1a/b*$^{(-/-)}$ mice, brain activity uptake was 2.5-fold higher compared to wild-type animals, whereas in *Bcrp1*$^{(-/-)}$ mice brain activity uptake was only 1.3-fold higher. *In vitro* autoradiography showed that 63% of [^{11}C]-**1** binding was displaceable by an excess of unlabeled **1**. As the signal obtained with [^{11}C]-**1** appeared to be specific for P-gp at the BBB, its utility for the visualization of cerebral P-gp merits further investigation.

Keywords

P-gp; elacridar; ^{11}C; PET; blood-brain barrier

[*]Corresponding author: Molecular Medicine, AIT Austrian Institute of Technology GmbH, 2444 Seibersdorf, Austria, Tel.: +43 50 550 3496. Fax: +43 50 550 3473. oliver.langer@ait.ac.at; and Department of Clinical Pharmacology, Medical University of Vienna, Währinger-Gürtel 18-20, 1090 Vienna, Austria, Tel.: +43 40400 2981. Fax: +43 40400 2998. oliver.langer@meduniwien.ac.at.
Bernd Dörner and Claudia Kuntner contributed equally to this study.

Supporting Information Available. Experimental and spectroscopic data for the non-key intermediates **2**, **3**, **7** and **8**. HPLC chromatogram of [^{11}C]-**1**. TACs for [^{11}C]-**1** PET scans during which **1** or tariquidar was administered. This material is available free of charge via the Internet at http://pubs.acs.org.

Europe PMC Funders Author Manuscripts

Introduction

The multidrug efflux transporter P-glycoprotein (P-gp[a], ABCB1) is highly expressed in the luminal membrane of vascular endothelial cells constituting the blood-brain barrier (BBB).[1] P-gp hinders brain uptake of lipophilic xenobiotics by active transport directly back into the vascular compartment acting as a protection mechanism. Apart from its well established role in mediating multidrug resistance of cancer cells [2], changes in P-gp function and expression are thought to be implicated in several neurologic disorders, such as epilepsy, depression, Parkinson's and Alzheimer's disease.[1]

Positron emission tomography (PET) imaging with radiolabeled substrates of P-gp, such as racemic [^{11}C]-verapamil,[3-5] (*R*)-[^{11}C]-verapamil,[6-8] [^{11}C]-loperamide [9] and [^{11}C]-*N*-desmethylloperamide [10, 11] has proved to be useful for studying P-gp function *in vivo*, both in animals and human subjects. Because currently available PET probes are high-affinity substrates for P-gp, they are efficiently kept out of the brain by P-gp-transport and therefore possess low brain uptake. Low brain uptake makes it difficult to use these probes for the mapping of regional differences in cerebral P-gp activity, which are expected to occur for example in medically refractory epilepsy.[1] A promising complementary approach to the use of radiolabeled substrates for assessing P-gp *in vivo* would be the use of radiolabeled inhibitors of P-gp which bind with nanomolar affinity to the pump without being transported. Such tracers are expected to give a signal increase rather than a reduction in brain regions that overexpress P-gp. A combined use of PET tracers based on P-gp inhibitors with radiolabeled transporter substrates, such as (*R*)-[^{11}C]-verapamil, might be particularly informative, as inhibitors would allow for assessing transporter distribution, whilst substrates assess transporter function.

Despite the fact that several potent P-gp inhibitors are known from the literature, such as the third-generation P-gp inhibitors elacridar (GF120918), tariquidar (XR9576), zosuquidar (LY335979) and laniquidar (R101933) (Fig. 1),[12] only two radiotracers based on P-gp inhibitors have been reported to date. In one recent study, ^{11}C-labeled laniquidar was evaluated in biodistribution experiments in rats, which revealed relatively low brain activity uptake (about 0.06 percent of the injected dose per gram tissue, %ID/g), which was enhanced after pre-treatment with the non-specific P-gp modulator cyclosporine A.[13] Another study reported on the ^{11}C-labeling and small-animal PET evaluation of 6,7-dimethoxy-2-{3-[4-methoxy-3,4-dihydro-2*H*-naphthalen-(1*E*)-ylidene]-propyl}-1,2,3,4-tetrahydro-isoquinoline (also named MC-18, Fig. 1), a potent P-gp inhibitor derived from tariquidar.[14]

In this study, we report the precursor synthesis, ^{11}C-labeling and small-animal PET evaluation of elacridar (**1**, Fig. 1), which is one of the most potent and selective P-gp inhibitors known to date.[15] We were able to demonstrate that [^{11}C]-**1** binds specifically to P-gp at the BBB, which makes [^{11}C]-**1** a promising candidate tracer for assessing the distribution of P-gp with PET.

Results

Chemistry and radiolabeling

The radiolabeling precursor of [^{11}C]-**1**, *O*-desmethyl-elacridar (**10**), was synthesized as outlined in Scheme 1. Acridone acid derivative **3** was demethylated using HBr/Ac_2O to give

[a]Abbreviations: BBB, blood-brain barrier; BCRP, breast cancer resistance protein; *Bcrp1*$^{(-/-)}$ mouse, BCRP knockout mouse; %ID/g, percent injected dose per gram tissue; *Mdr1a/b*$^{(-/-)}$ mouse, P-gp knockout mouse; PET, positron emission tomography; P-gp, P-glycoprotein; SPE, solid-phase extraction; TAC, time-activity curve

4.[16] As the direct coupling of **4** with 6,7-dimethoxy-2-(4-aminophenethyl)-1,2,3,4-tetrahydroisochinoline (**8**) was not successful,[17] protection of the free phenolic function became necessary. In a first attempt, an acetyl protective group was used, but was not stable enough for the following coupling reaction. The benzylic group was found to be the preferred protective group for the phenol. Treatment of **4** with benzyl chloride resulted in the formation of the benzyl ester **5** of the corresponding benzyl-protected phenol **6**. The benzyl ester was selectively cleaved using a mixture of aq. LiOH and MeOH to afford benzyloxy acridone carboxylic acid **6**. Compound **6** was then coupled with **8** [17] to give compound **9**, the benzylic derivative of **1**. The benzyl protective group was finally cleaved by catalytic hydrogenation to yield **10**. It was also attempted to synthesize a derivative of **1** with a free phenolic OH function in the aminophenethyl isoquinoline part of the molecule. However, all attempts to couple the corresponding desmethyl isoquinoline derivative [18, 19] with 4-nitrophenethyl bromide failed and selective protection of the phenol group was also not successful.

For the ^{11}C-labeling of **1**, compound **10** was reacted with [^{11}C]-methyl triflate in acetone containing aq. NaOH (Scheme 1). [^{11}C]-**1**, ready for i.v. injection, was obtained in a decay-corrected radiochemical yield of 5±1% (n=14) based on [^{11}C]-CH_4, in a total synthesis time of 40 min. Radiochemical purity was greater than 98% (see supporting information for representative HPLC chromatogram) and the specific activity at the end of synthesis was 140±32 GBq/μmol (n=10). The identity of [^{11}C]-**1** was confirmed by HPLC co-injection with unlabeled **1** (see supporting information for representative HPLC chromatogram).

Small-animal PET in rats and mice

[^{11}C]-**1** was evaluated in naïve rats using a double-scan paradigm that we had previously used for (*R*)-[^{11}C]-verapamil.[6] The study outline is shown in Fig. 2. In the first PET scan, brain uptake of activity was low. Peak brain uptake was 0.23±0.01 %ID/g at 0.6 min after tracer injection. At 18 min after tracer injection brain uptake had declined to 0.07±0.00 %ID/g. In response to administration of unlabeled **1** (5 mg/kg) at 60 min after radiotracer injection, there was a steep increase in brain activity uptake reaching 0.28±0.03 %ID/g at 130 min after tracer injection, whereas blood activity levels remained unchanged (Fig. 2). When tariquidar (3 mg/kg) instead of **1** was injected during scan 1, brain activity levels remained unchanged until the end of the scan (see supporting information). In the second PET scan performed after injection of unlabeled **1**, brain activity uptake was 5.4 times higher as compared to scan 1 (0.40±0.08 *versus* 0.07±0.00 %ID/g for scan 2 and scan 1, respectively, both at 18 min after tracer injection, p=0.002) with similar blood activity levels as in scan 1 (Fig. 2). In Fig. 3 representative PET summation images are shown for both scans. In scan 1 (upper row), brain activity uptake was lower and in scan 2 (lower row) brain activity uptake was several-fold higher than activity uptake in surrounding head tissue.

Radiolabeled metabolites of [^{11}C]-**1** in plasma were assessed by a solid-phase extraction (SPE) assay. At 20 min after [^{11}C]-**1** injection, 14±11% of total plasma activity was recovered in SPE fractions 1 and 2 and 85±11% in fraction 3 (mean values of 20-min samples collected in scan 1 and 2 are stated). At 60 min after second [^{11}C]-**1** injection, 18±12% of total plasma activity was in fractions 1 and 2, and 82±12% in fraction 3. Fraction 3 was further analyzed by radio-HPLC. Representative HPLC chromatograms for samples collected at 20 min and 60 min after tracer injection are shown in Fig. 4. Whereas for the 20 min sample unchanged [^{11}C]-**1** was the only radiolabeled species detectable in fraction 3, an unidentified polar radiolabeled species was seen in the 60 min sample that accounted for about 30% of total activity.

In Fig. 5, PET summation images and brain time-activity curves (TACs) of [^{11}C]-**1** in wild-type, P-gp knockout (*Mdr1a/b*$^{(-/-)}$) and BCRP knockout (*Bcrp1*$^{(-/-)}$) mice are shown. In *Mdr1a/b*$^{(-/-)}$ and *Bcrp1*$^{(-/-)}$ mice, brain activity levels were 2.5-fold (p=0.0003) and 1.3-fold (p=0.01) higher than in wild-type mice (1.80±0.15, 0.90±0.08 and 0.72±0.04 %ID/g for *Mdr1a/b*$^{(-/-)}$, *Bcrp1*$^{(-/-)}$and wild-type mice, respectively, all at 18 min after tracer injection). Blood activity levels in *Mdr1a/b*$^{(-/-)}$ and *Bcrp1*$^{(-/-)}$ mice did not differ significantly from wild-type mice, although there was a trend for lower values in *Mdr1a/b*$^{(-/-)}$ mice (0.64±0.30, 0.89±0.43 and 0.97±0.42 %ID/g for *Mdr1a/b*$^{(-/-)}$, *Bcrp1*$^{(-/-)}$and wild-type mice, respectively, all at 20 min after tracer injection, p>0.30).

Interestingly, brain concentration of [^{11}C]-**1** was about 10-fold higher in wild-type mice as compared to naïve rats (0.72±0.04 and 0.07±0.00 %ID/g for mice and rats, respectively, both at 18 min after tracer injection). However, blood activity levels were also several-fold higher in wild-type mice than in rats (0.97±0.42 and 0.02±0.01 %ID/g for wild-type mice and rats, respectively, both at 20 min after tracer injection).

In vitro autoradiography

Fig. 6 shows *in vitro* autoradiograms of rat brain sections incubated with [^{11}C]-**1**. Brain sections that were co-incubated with a mixture of [^{11}C]-**1** and unlabeled **1** (1 μM) showed 63±9% reduction in radioactive signal as compared to brain sections that were incubated with [^{11}C]-**1** alone.

Discussion

The aim of this study was the development of a highly selective and potent radiolabeled P-gp inhibitor for imaging the distribution of cerebral P-gp with PET. **1** (Fig. 1) was selected as a candidate compound because there is ample evidence from pre-clinical studies that **1** very potently inhibits P-gp function at the BBB as reflected by increased brain accumulation of P-gp substrate drugs.[20, 21] Moreover, **1** inhibits *in vitro* P-gp-mediated transport of daunorubicin in rat hepatocyte canalicular membrane vesicles in the low nanomolar concentration range (inhibition constant K_i 35 nM) [22] and has been shown to be a non-transported inhibitor of P-gp.[23, 24] **1** also inhibits breast cancer resistance protein (BCRP, ABCG2), another efflux transporter expressed at the BBB, at comparable concentrations as it inhibits P-gp.[25] However, in contrast to first- and second-generation P-gp inhibitors, **1** does not inhibit multidrug resistance-associated proteins (MRPs) such as MRP1.[1] **1** has entered clinical trials for reverting multidrug resistance in cancer.[2, 26] We considered it of advantage to select a compound for PET tracer development that has advanced to clinical trials, as such compounds can be expected to be safe and optimized in terms of absorption, distribution, metabolism and toxicity (ADMET) properties. In addition, **1** contains three OCH_3 groups, which allows for straightforward ^{11}C-labeling *via* ^{11}C-methylation without changing the chemical structure of the molecule (Fig. 1).

In this study, the *in vivo* specificity of [^{11}C]-**1** for P-gp was assessed by small-animal PET imaging using two different approaches. First, we performed PET experiments in naïve rats before and after administration of unlabeled **1**. Second, we performed PET experiments in *Mdr1a/b*$^{(-/-)}$ and *Bcrp1*$^{(-/-)}$ mice that do not express the putative imaging targets of [^{11}C]-**1**.

The behavior of [^{11}C]-**1** in rats was surprising in that brain activity started to rise significantly in immediate response to injection of unlabeled **1** (Fig. 2), but not in response to injection of tariquidar (see supporting information). Moreover, in the second PET scan, which was performed at 2 h after injection of unlabeled **1**, brain activity uptake was 5.4-fold higher as compared to scan 1. This *in vivo* behavior is comparable to what we had previously seen for the P-gp substrate radiotracer (*R*)-[^{11}C]-verapamil using a comparable

study set-up.[6] For (*R*)-[^{11}C]-verapamil, brain activity uptake was about 12-fold increased in the second PET scan performed at 2 h after administration of 15 mg/kg tariquidar. Interestingly, similar findings were reported in biodistribution experiments with [^{11}C]-laniquidar in rats, in which brain uptake of activity was 6-9 fold higher after pretreatment with cyclosporine A (50 mg/kg, i.v.).[13] For [^{11}C]-MC-18 (Fig. 1), on the other hand, brain activity uptake in rats was reduced by about 30% compared to baseline scans following administration of unlabeled MC-18 (15 mg/kg).[14]

At first glance the behavior of [^{11}C]-**1** might correspond to that of a P-gp substrate rather than a non-transported P-gp inhibitor. However, it has been shown before that **1** does not stimulate adenosine triphosphatase (ATPase) activity and has a basolateral-apical (B-A) to apical-basolateral (A-B) concentration ratio <2 in monolayer Caco-2 cell transport assays which suggests that **1** is not a substrate of P-gp.[24, 27] When considering the physiologic function of P-gp, which acts as a gate keeper at the BBB preventing influx of P-gp substrates into brain tissue,[28] it seems likely that a tracer dose of [^{11}C]-**1** is hindered from crossing the BBB by high-affinity binding to P-gp. This is also in line with our PET data in *Mdr1a/b*$^{(-/-)}$ mice, which lacked P-gp and displayed high brain uptake of the radioactive probe (Fig. 5). Further support in favor of the assumption that [^{11}C]-**1** behaves *in vivo* as a non-transported P-gp inhibitor and not as a substrate is given by the observation that tariquidar (3 mg/kg), another non-transported P-gp inhibitor which has been shown to bind to a distinct P-gp binding site[23], exerted no effect on [^{11}C]-**1** TACs during scan 1 (see supporting information). When given during a PET scan with the P-gp substrate (*R*)-[^{11}C]-verapamil, on the other hand, the employed tariquidar dose (3 mg/kg) caused a pronounced increase in brain activity uptake (see supporting information). The effect of 3 mg/kg tariquidar on brain uptake of (*R*)-[^{11}C]-verapamil and the lack of such an effect on brain uptake of [^{11}C]-**1** does not necessarily mean that tariquidar is unable to allosterically modulate binding of **1** to P-gp [23], it could just mean that the potency is lower than for inhibition of (*R*)-[^{11}C]-verapamil transport.

We hypothesize that administration of unlabeled **1** at a dose which completely inhibits cerebral P-gp [29] might have displaced [^{11}C]-**1** from its P-gp binding site resulting in unhindered passive diffusion of unmetabolized [^{11}C]-**1** from blood into brain. As brain activity levels rose above blood levels during the late part of scan 1 (Fig. 2), it can be assumed that diffusion into brain was driven by one or more so far unknown binding processes in brain, possibly P-gp expressed in astroglial cells and neurons or some intra- or extracellular binding sites unrelated to P-gp.[1] The gate keeper function of P-gp under unblocked conditions can be considered as an advantage regarding the utility of [^{11}C]-**1** for PET imaging, as it prevents brain entry and thus non-specific binding of the highly lipophilic probe (calculated log*P* (o/w) 4.2, MOE, Chemical Computing Group, Montreal, Canada) in brain tissue, which would mask P-gp-specific binding. In the same context, the metabolic stability of [^{11}C]-**1** can be considered as an advantage, as radiolabeled metabolites of [^{11}C]-**1**, if present, might show P-gp independent brain uptake and thereby potentially contaminate the P-gp specific signal of [^{11}C]-**1**. Our data are intriguing in that they exemplify how the biodistribution of a microdose of a drug can substantially differ from that of a therapeutic dose (Fig. 3).[30]

In order to further substantiate our assumption of P-gp specific *in vivo* binding of [^{11}C]-**1**, we performed *in vitro* autoradiography of rat brain sections with [^{11}C]-**1**. In these experiments, co-incubation with unlabeled **1** resulted in a 63% decrease of radiotracer binding (Fig. 6), as opposed to the increase that we had seen in the *in vivo* experiments (Fig. 3). This suggests saturable binding of [^{11}C]-**1** to rat brain slices, but does not prove by itself that this binding site is located on cerebral P-gp. As the BBB does not act as gate keeper in

the autoradiography set-up, we speculate that displacement of P-gp binding of [^{11}C]-**1** might have caused the signal reduction in these experiments.

Specific interaction of [^{11}C]-**1** with P-gp expressed at the BBB was further demonstrated by PET experiments in wild-type, *Mdr1a/b*$^{(-/-)}$ and *Bcrp1*$^{(-/-)}$ mice (Fig. 5). In *Mdr1a/b*$^{(-/-)}$ mice, brain activity levels were 2.5-fold higher compared to wild-type mice, at comparable blood activity levels. In *Bcrp1*$^{(-/-)}$ mice, on the other hand, brain activity levels were only 1.3-fold higher than in wild-type animals. This suggests that P-gp is quantitatively more important than BCRP in limiting brain entry of [^{11}C]-**1**.

Interestingly, the brain concentration of [^{11}C]-**1** was about 10-fold higher in wild-type mice than in rats. This difference in brain activity concentration can most likely be explained by the several-fold higher blood activity levels measured in mice compared to rats. The exact reasons for these considerable differences in blood clearance of [^{11}C]-**1** in the two studied species are unclear at present.

Conclusion

We synthesized the radiolabeled third-generation P-gp inhibitor [^{11}C]-**1** and evaluated it by means of small-animal PET imaging and *in vitro* autoradiography. [^{11}C]-**1** was found to display high metabolic stability and displaceable *in vitro* binding to rat brain slices. *In vivo*, brain uptake of [^{11}C]-**1** appeared to be specific for P-gp expressed at the BBB as reflected by significant changes in brain activity uptake following administration of unlabeled **1** to rats. Experiments in *Mdr1a/b*$^{(-/-)}$ and *Bcrp1*$^{(-/-)}$ mice suggested that the contribution of BCRP to limiting brain entry of [^{11}C]-**1** is small as compared to that of P-gp. The usefulness of [^{11}C]-**1** for the visualization and quantification of cerebral P-gp merits further investigation including experiments in animal models of P-gp overexpression.

Experimental section

General

Unless otherwise stated, all chemicals were of analytical grade and obtained from Sigma-Aldrich Chemie GmbH (Schnelldorf, Germany), Merck (Darmstadt, Germany) or TCI Europe (Zwijndrecht, Belgium) and used without further purification. Isofluran was obtained from Baxter VertriebsGmbH (Vienna, Austria). The hydrochloride salt of **1** was obtained from Glaxo SmithKline (Research Triangle Park, NC, USA) and tariquidar dimesylate from Xenova Ltd. (Slough, Berkshire, UK). For administration, **1** hydrochloride was dissolved freshly on each experimental day in a 20% aq. EtOH solution and injected at a volume of 2 or 4 mL/kg in rats and mice, respectively. Tariquidar was dissolved in 2.5% (g/v) aqueous dextrose solution and injected at a volume of 3 mL/kg into rats. [^{11}C]-CH_4 was produced *via* the ^{14}N(p,α)^{11}C nuclear reaction by irradiating nitrogen gas containing 10% hydrogen using a PETtrace cyclotron equipped with a CH_4 target system (GE Healthcare, Uppsala, Sweden). Typically, irradiation duration of 30 min with a beam current of 25 μA yielded 30-35 GBq of [^{11}C]-CH_4. [^{11}C]-CH_3I was prepared *via* the gas-phase method [31] in a TRACERlab FX C Pro synthesis module (GE Healthcare) and converted into [^{11}C]-methyl triflate by passage through a column containing silver-triflate impregnated graphitized carbon.[32] ^{1}H- and ^{13}C-NMR spectra were recorded on a Bruker Advance DPx200 (200 and 50 MHz). Chemical shifts are reported in δ units (ppm) relative to Me_4Si line as internal standard (s, bs, d, m, Cq for singlet, broad singlet, doublet, multiplet and quartenary carbon, respectively) and *J* values are reported in Hertz. Mass spectra (MS) were obtained with a Shimadzu (GC-17A; MS-QP5050A) spectrometer. Purity of compounds **4**, **5**, **6**, **9** and **10** was established by analytical reversed-phase high-performance liquid chromatography (HPLC) confirming a purity >95%.

Animals

Adult female Sprague Dawley rats weighing 270-290 g were obtained from Harlan Netherlands (Horst, Netherlands). Female FVB (wild-type), *Mdr1a/b*$^{(-/-)}$ and *Bcrp1*$^{(-/-)}$ mice weighing 25-30 g were purchased from Taconic Inc. (Germantown, NY, USA). The study was approved by the local Animal Welfare Committee and all study procedures were performed in accordance with the Austrian Animal Experiments Act. Animals had access to food and H_2O *ad libitum* and were kept under a 12 h light/dark cycle.

5-Hydroxyacridone-4-carboxylic acid (4)

To a suspension of compound **3** (2.69 g, 10 mmol), which had been prepared from 2-(2-carboxyphenylamino)-3-methoxybenzoic acid (**2**) as described in the literature (see supporting information),[17] in HBr (48%, 60 mL) Ac_2O (30 mL) was added. The mixture was refluxed for 24 h. The solid was then filtered, washed with H_2O and cold EtOH and dried under vacuum to give **4** as an orange powder (2.47 g, 96.9% theoretical yield).

MS *m/z* 255 (92%, M^+), 237 (82%), 209 (100%), 153 (29%), 118 (23%). ^{1}H-NMR (d_6-DMSO): δ 7.08-7.44 (m, 3H), 7.64-7.76 (m, 1H), 8.40-8.60 (m, 2H), 10.91 (s, 1H), 12.16 (s, 1H); ^{13}C-NMR (d_6-DMSO): δ 114.9 (Cq), 115.6 (CH), 116.2 (CH), 120.0 (CH), 121.4 (Cq), 121.5 (Cq), 121.9 (CH), 130.6 (Cq), 132.5 (CH), 136.7 (CH), 140.4 (Cq), 145.7 (Cq), 169.1 (COOH), 176.4 (CO)

5-(Benzyloxy)acridone-4-carboxylic acid benzyl ester (5)

To a suspension of compound **4** (0.925 g, 3.6 mmol) and K_2CO_3 (4.98 g, 36 mmol, 10 eq.) in dry DMF (35 mL), benzyl chloride (1.035 mL, 9 mmol, 2.5 eq.) was added. The mixture was stirred for 10 min at room temperature (rt) and then stirred at 50°C for 48 h. The solution was poured on ice H_2O and the obtained solid was filtered, washed with H_2O and dried under vacuum to afford the title compound as a yellow solid (1.252 g, 79.9% theoretical yield).

MS *m/z* 435 (7%, M^+), 359 (7%), 344 (6%), 91 (100%), 65 (10%). ^{1}H-NMR ($CDCl_3$): δ 5.31 (s, 2H, OCH_2), 5.41 (s, 2H, OCH_2), 7.11-7.26 (m, 3H), 7.30-7.53 (m, 8H), 7.55-7.68 (m, 2H), 7.90-8.06 (m, 1H), 8.31-8.50 (m, 1H), 8.58-8.80 (m, 1H), 12.18 (s, 1H); ^{13}C-NMR ($CDCl_3$): δ 67.0 (CH2), 70.5 (CH2), 113.6 (CH), 114.2 (Cq), 118.3 (CH), 119.9 (CH), 121.4 (CH), 122.0 (Cq), 122.3 (Cq), 126.8 (2xCH), 128.0 (CH), 128.5 (2xCH), 128.6 (2xCH), 128.7 (2xCH), 131.7 (Cq), 133.8 (CH), 135.5 (Cq), 136.2 (Cq), 136.5 (CH), 140.9 (Cq), 146.7 (Cq), 167.2 (COO), 177.6 (CO)

5-(Benzyloxy)acridone-4-carboxylic acid (6)

Compound **5** (2.17 g, 5 mmol) was suspended in a mixture of MeOH and 2 M aq. LiOH (1/1, v/v, 400 mL). The suspension was heated to reflux for 2 h, cooled to rt, acidified with HCl (2 M) and further cooled on ice. The obtained solid was filtered, washed with H_2O and cold EtOH and dried under vacuum to afford the title compound as a yellow solid (1.543 g, 89.4% theoretical yield).

MS *m/z* 345 (14%, M^+), 254 (11%), 236 (27%), 91 (100%), 65 (12%). ^{1}H-NMR (d_6-DMSO): δ 5.40 (s, 2H, OCH_2), 7.20-7.71 (m, 8H), 7.75-7.90 (m, 1H), 8.39-8.59 (m, 2H), 12.5 (s, 1H); ^{13}C-NMR (d_6-DMSO): δ 70.3 (CH_2), 114.3 (CH), 115.4 (Cq), 117.3 (CH), 120.3 (CH), 121.1 (Cq) , 121.5 (Cq), 121.6 (CH), 127.4 (2CH), 127.9 (CH), 128.5 (2CH), 131.1 (Cq), 132.2 (CH), 136.3 (Cq), 136.7 (CH), 140.5 (Cq), 146.5 (Cq), 169.3 (COOH), 176.3 (CO)

Benzylic derivative of 1 (9)

To a solution of compound **6** (1.036 g, 3 mmol) and 6,7-dimethoxy-2-(4-aminophenethyl)-1,2,3,4-tetrahydroisochinoline (**8**, 0.937 g, 3 mmol, 1 eq.), which had been prepared from 6,7-dimethoxy-2-(4-nitrophenethyl)-1,2,3,4-tetrahydroisochinoline (**7**) according to the literature (see supporting information),[17] in dry DMF (12 mL) *O*-(benzotriazol-1-yl)-*N,N,N',N'*-tetramethyluronium tetrafluoroborate (TBTU, 1.011 g, 3.15 mmol, 1.05 eq.) and Et_3N (0.873 mL, 6.3 mmol, 2.1 eq.) were added. The solution was stirred for 2 h at rt, then a mixture of MeOH and isopropanol (1/1, v/v, 12 mL) was added. The mixture was stirred for additional 30 min. The obtained slurry was filtered, washed with MeOH and H_2O and dried under vacuum to afford the title compound as a yellow solid (1.457 g, 76% theoretical yield).

ESI/MS *m/z* 640 (100%, $M+1^+$), 639 (23%, M^+), 638 (50%, $M-1^+$). ^{1}H-NMR ($CDCl_3$): δ 2.75-3,08 (m, 8H), 3.70 (s, 2H), 3.84 (s, 3H, OCH_3), 3.85 (s, 3H, OCH_3), 5.32 (s, 2H, OCH_2), 6.55 (s, 1H), 6.61 (s, 1H), 6.90-7.52 (m, 9H), 7.55-7.80 (m, 4H), 7.89-8.06 (m, 2H), 8.40-8.63 (m, 2H), 12.35 (s, 1H); ^{13}C-NMR ($CDCl_3$): δ 28.5 (CH_2), 33.4 (CH_2), 51.0 (CH_2), 55.6 (CH_2), 55.9 (2×OCH_3), 60.0 (CH_2), 70.5 (CH_2), 109.4 (CH), 111.3 (CH), 113.6 (CH), 118.2 (CH), 119.1 (Cq), 119.6 (CH),120.8 (2×CH), 121.3 (CH), 121.8 (Cq), 122.5 (Cq), 126.0 (Cq), 126.1 (Cq), 126.7 (2×CH), 127.9 (CH), 128.6 (2×CH), 129.3 (2×CH), 131.4 (CH), 131.7 (CH), 132.0 (Cq), 135.9 (Cq), 136.3 (Cq), 137.0 (Cq), 140.0 (Cq), 146.8 (Cq), 147.2 (Cq), 147.6 (Cq), 166.4 (CON), 177.9 (CO)

O-Desmethyl-elacridar (10)

A suspension of compound **9** (0.959 g, 1.5 mmol) and Pd/C catalyst (10% w/w, 0.096 g) in EtOH (330 mL) was stirred at rt under hydrogen gas until hydrogen uptake was finished. The mixture was filtered and the catalyst was washed several times with hot EtOH. The combined solutions were evaporated and dried under vacuum to give compound **10** as a yellow solid (0.436 g, 52.9% theoretical yield).

ESI/MS *m/z* 549 (37%, M^+), 548 (100%), 546 (18%). ^{1}H-NMR (d_6-DMSO): δ 2.67-3.00 (m, 8H), 3.61 (s, 2H, CH_2), 3.76 (s, 6H, 2×OCH_3), 6.72 (s, 2H), 7.08-7.56 (m, 5H), 7.66-7.85 (m, 3H), 8.42-8.65 (m, 2H), 10.78 (bs, 1H), 12.26 (bs, 1H); ^{13}C-NMR (d_6-DMSO, 50 Hz): δ 28.3 (CH_2), 32.4 (CH_2), 50.5 (CH_2), 55.0 (CH_2), 55.3 (OCH_3), 55.4 (OCH_3), 59.5 (CH_2), 109.9 (CH), 111.6 (CH), 114.9 (CH), 115.9 (CH), 118.8 (Cq), 119.5 (CH), 121.2 (CH), 121.3 (Cq), 121.4 (Cq), 121.7 (CH), 125.8 (Cq), 126.6 (Cq), 128.8 (CH), 130.7 (CH), 131.1 (Cq), 133.6 (CH), 136.2 (Cq), 136.5 (Cq), 139.8 (Cq), 146.7 (Cq), 146.8 (Cq), 147.0 (Cq), 166.5 (CON), 176.5 (CO)

[^{11}C]-elacridar ([^{11}C]-1)

Using a TracerLab FXC Pro synthesis module [^{11}C]-methyl triflate was bubbled through a solution of **10** (0.3 mg, 0.53 μmol) in acetone (0.5 mL) containing aq. NaOH (0.3 M, 10 μL, 3 μmol, 5.7 eq.). After heating for 4 min at 60°C, the reaction mixture was cooled (25°C), diluted with H_2O (0.5 mL) and injected into the built-in HPLC system. A Chromolith Performance RP 18-e (100-4.6 mm) column (Merck KGaA, Darmstadt, Germany) was eluted at flow rate of 5 mL/min with CH_3CN/MeOH/ammonium acetate buffer (0.2 M, pH 5.0) (225/50/725, v/v/v). The HPLC eluate was monitored in series for radioactivity and ultraviolet (UV) absorption at a wavelength of 227 nm. On this system radiolabeling precursor **10** and product [^{11}C]-**1** eluted with retention times of 3 min and 7-9 min, respectively. The product fraction was diluted with H_2O (100 mL) and passed over a C18 Sep-Pak Plus cartridge (Waters Corporation, Milford, MA, USA), which had been pre-activated with EtOH (5 mL) and H_2O (10 mL). The cartridge was then washed with H_2O (10 mL) followed by elution of [^{11}C]-**1** from the cartridge with EtOH (3 mL). The EtOH

was then removed by heating at 100°C under a stream of argon and the product formulated in a mixture of 0.9% aq. saline/EtOH/polyethylene glycol 300 (50/15/35, v/v/v) at an approximate concentration of 370 MBq/mL for i.v. injection into animals. Radiochemical and chemical purity and specific activity of [^{11}C]-**1** was determined by analytical radio-HPLC using a Nucleosil 100-3 C18 column (3 μm, 3.00×125 mm, Macherey-Nagel, Düren, Germany) eluted with CH_3CN/MeOH/ammonium acetate buffer (0.2 M, pH 5.0) (350/78/572, v/v/v) at a flow rate of 0.5 mL/min. UV detection was performed at a wavelength of 227 nm. The retention time of [^{11}C]-**1** was about 15-17 min on this HPLC system (see supporting information).

Small-animal PET imaging and PET data analysis

Prior to each experiment, the animals were placed into an induction box and anesthetized with 2.5% isoflurane. When unconscious, the animals were taken from the box and kept under anesthesia with 1.5-2% isoflurane administered *via* a mask during the whole experiment. Animals were warmed throughout the whole experiment at around 38°C. Rats were implanted with catheters into the femoral artery (for blood sampling) and vein (for administration of **1** or tariquidar, and [^{11}C]-**1**). In mice, the lateral tail vein was used for radiotracer administration. The animals were positioned in the imaging chamber and [^{11}C]-**1** (rats: 118±40 MBq in a volume of about 0.3 mL, mice: 42±6 MBq in a volume of about 0.1 mL) was administered as an i.v. bolus over approximately 30 s. At the start of radiotracer injection, dynamic PET imaging was initiated using a microPET Focus220 scanner (Siemens, Medical Solutions, Knoxville, TN, USA).

Rats underwent paired PET scans with [^{11}C]-**1** (see study outline in Fig. 2). At 60 min after start of scan 1, unlabeled **1** (5 mg/kg) was injected as an i.v. bolus over approximately 20 s, which was followed by further 90 min of PET data acquisition. Scan 2 with [^{11}C]-**1** was performed at 2 h after injection of unlabeled **1** (Fig. 2). An additional group of rats (n=3) underwent single 150-min [^{11}C]-**1** PET scans, during which tariquidar (3 mg/kg) was injected at 60 min after start of the scan. For the rat experiments, 5-μL arterial blood samples were withdrawn manually with pre-weighted micropipettes from the femoral artery (approximately every 5 s) during the first 3 min after radiotracer injection, followed by further 10-μL samples taken at 5, 10, 20, 30, 40, 50, 60, 70, 80 and 90 min (last three time points only for scan 1). Moreover, one larger blood sample (0.6 mL) was collected into an heparinized vial at 20 min (scan 1 and scan 2) after tracer injection in order to determine metabolism of [^{11}C]-**1** (see below) and the plasma-to-blood ratio of activity. At the end of scan 2, rats were sacrificed. A terminal blood sample (5 mL) was collected and radiolabeled metabolites of [^{11}C]-**1** in plasma were determined using a SPE assay [33] that we had previously used for the analysis of (*R*)-[^{11}C]-verapamil in rat plasma.[6] In brief, plasma was spiked with unlabeled **1** and acidified with 5M aq. HCl (10 μL) and loaded on a Sep-Pak vac tC18 cartridge (Waters Corporation, Milford, USA), which had been pre-activated with MeOH (3 mL) and H_2O (5 mL). The cartridge was first washed with H_2O (5 mL) and then eluted with MeOH (4 mL) followed by ammonium acetate buffer (0.2 M, pH 5.0, 4 mL). Radioactivity in all three fractions (plasma, H_2O, MeOH/buffer) was quantified in a 1-detector Wallac gamma counter (Perkin Elmer Instruments, Wellesley, MA, USA), which was cross-calibrated with the PET camera. Radioactivity in the plasma and H_2O fractions (fraction 1 and 2) contained hydrophilic radiolabeled metabolites of [^{11}C]-**1**, whereas unchanged [^{11}C]-**1** and lipophilic radiolabeled metabolites were found in the MeOH/buffer fraction (fraction 3). Fraction 3 was further analyzed by HPLC using the same chromatographic conditions as described above for the semipreparative HPLC purification of [^{11}C]-**1**.

Mice underwent only single 60-min PET scans with [^{11}C]-**1**. At 20 min after radiotracer injection one venous blood sample (approximately 10 μL) was collected. During each scanning session, two mice were examined simultaneously. All blood samples were weighted and counted for activity in the gamma counter. Blood activity data were corrected for radioactive decay and expressed as %ID/g.

PET images were reconstructed by Fourier rebinning followed by 2-dimensional filtered back projection with a ramp filter. The standard data correction protocol (normalization, attenuation, decay correction and injection decay correction) was applied to the data. As P-gp is ubiquitous in brain and as we were interested in global binding of [^{11}C]-**1** in brain, whole brain was manually outlined on multiple planes of the PET summation images using the image analysis software Amide [34] and TACs, expressed in units of %ID/g, were calculated.

For all outcome parameters, differences between scans before and after inhibitor administration were tested with a two-tailed paired Student's *t*-test. For unpaired data, a two-tailed Student's *t*-test was used. The level of statistical significance was set to $p<0.05$.

In vitro autoradiography

One naïve Sprague Dawley rat was decapitated under deep anaesthesia, whole brain was immediately removed, embedded in Tissue Freezing Medium (Jung, Nussloch, Germany) and snap frozen in liquid N_2. Brain was cut in coronal 10 μm slices with a cryostat (Microm HM 550, Walldorf, Germany) and mounted on HistoBond slides (Marienfeld, Lauda-Königshofen, Germany). Brain slices were pre-incubated with phosphate-buffered saline (PBS) for 10 min. Subsequently the slices were incubated in PBS for 30 min with either [^{11}C]-**1** alone (about 10 MBq) or [^{11}C]-**1** and unlabeled **1** (1 μM) and washed two times for 5 min each with 20% (v/v) EtOH in PBS to remove nonspecifically bound radiotracer. The slides were then exposed for 2 h to a multisensitive phosphor screen (type:MS, Perkin Elmer Life Sciences) which was afterwards scanned with a phosphor imager (Cyclone, Packard Instruments, Meriden, CN, USA).

Supplementary Material

Refer to Web version on PubMed Central for supplementary material.

Acknowledgments

The research leading to these results has received funding from the European Community's Seventh Framework Programme (FP7/2007-2013) under grant agreement number 201380 ("Euripides") and from the Austrian Science Fund (FWF) project "Transmembrane Transporters in Health and Disease" (SFB F35). The authors thank Thomas Filip and Maria Zsebedics (Seibersdorf Laboratories GmbH) for their skillful help with laboratory animal handling, Florian Bauer (University of Vienna) for technical assistance and the staff of the radiochemistry laboratory (Seibersdorf Laboratories GmbH) for continuous support. Elacridar hydrochloride was kindly provided by Glaxo SmithKline (Research Triangle Park, NC, USA) and tariquidar dimesylate by Xenova Ltd. (Slough, Berkshire, UK).

References

1. Löscher W, Potschka H. Role of drug efflux transporters in the brain for drug disposition and treatment of brain diseases. Prog. Neurobiol. 2005; 76(1):22–76. [PubMed: 16011870]
2. Szakacs G, Paterson JK, Ludwig JA, Booth-Genthe C, Gottesman MM. Targeting multidrug resistance in cancer. Nat. Rev. Drug Discov. 2006; 5(3):219–234. [PubMed: 16518375]
3. Hendrikse NH, Schinkel AH, de Vries EG, Fluks E, Van der Graaf WT, Willemsen AT, Vaalburg W, Franssen EJ. Complete in vivo reversal of P-glycoprotein pump function in the blood-brain

barrier visualized with positron emission tomography. Br. J. Pharmacol. 1998; 124(7):1413–1418. [PubMed: 9723952]

4. Sasongko L, Link JM, Muzi M, Mankoff DA, Yang X, Collier AC, Shoner SC, Unadkat JD. Imaging P-glycoprotein transport activity at the human blood-brain barrier with positron emission tomography. Clin. Pharmacol. Ther. 2005; 77(6):503–514. [PubMed: 15961982]
5. Brunner M, Langer O, Sunder-Plassmann R, Dobrozemsky G, Müller U, Wadsak W, Krcal A, Karch R, Mannhalter C, Dudczak R, Kletter K, Steiner I, Baumgartner C, Müller M. Influence of functional haplotypes in the drug transporter gene ABCB1 on central nervous system drug distribution in humans. Clin. Pharmacol. Ther. 2005; 78(2):182–190. [PubMed: 16084852]
6. Bankstahl JP, Kuntner C, Abrahim A, Karch R, Stanek J, Wanek T, Wadsak W, Kletter K, Müller M, Löscher W, Langer O. Tariquidar-induced P-glycoprotein inhibition at the rat blood-brain barrier studied with (*R*)-^{11}C-verapamil and PET. J. Nucl. Med. 2008; 49(8):1328–1335. [PubMed: 18632828]
7. Lubberink M, Luurtsema G, van Berckel BN, Boellaard R, Toornvliet R, Windhorst AD, Franssen EJ, Lammertsma AA. Evaluation of tracer kinetic models for quantification of P-glycoprotein function using (*R*)-[(^{11})C]verapamil and PET. J. Cereb. Blood Flow Metab. 2007; 27(2):424–433. [PubMed: 16757979]
8. Langer O, Bauer M, Hammers A, Karch R, Pataraia E, Koepp MJ, Abrahim A, Luurtsema G, Brunner M, Sunder-Plassmann R, Zimprich F, Joukhadar C, Gentzsch S, Dudczak R, Kletter K, Müller M, Baumgartner C. Pharmacoresistance in epilepsy: a pilot PET study with the P-glycoprotein substrate *R*-[^{11}C]verapamil. Epilepsia. 2007; 48(9):1774–1784. [PubMed: 17484754]
9. Zoghbi SS, Liow JS, Yasuno F, Hong J, Tuan E, Lazarova N, Gladding RL, Pike VW, Innis RB. ^{11}C-loperamide and its N-desmethyl radiometabolite are avid substrates for brain permeability-glycoprotein efflux. J. Nucl. Med. 2008; 49(4):649–656. [PubMed: 18344435]
10. Liow JS, Kreisl W, Zoghbi SS, Lazarova N, Seneca N, Gladding RL, Taku A, Herscovitch P, Pike VW, Innis RB. P-Glycoprotein Function at the Blood-Brain Barrier Imaged Using 11C-N-Desmethyl-Loperamide in Monkeys. J. Nucl. Med. 2009; 50(1):108–115. [PubMed: 19091890]
11. Seneca N, Zoghbi SS, Liow JS, Kreisl W, Herscovitch P, Jenko K, Gladding RL, Taku A, Pike VW, Innis RB. Human Brain Imaging and Radiation Dosimetry of ^{11}C-N-Desmethyl-Loperamide, a PET Radiotracer to Measure the Function of P-Glycoprotein. J. Nucl. Med. 2009; 50(5):807–813. [PubMed: 19372478]
12. Wang RB, Kuo CL, Lien LL, Lien EJ. Structure-activity relationship: analyses of p-glycoprotein substrates and inhibitors. J. Clin. Pharm. Ther. 2003; 28(3):203–228. [PubMed: 12795780]
13. Luurtsema G, Schuit RC, Klok RP, Verbeek J, Leysen JE, Lammertsma AA, Windhorst AD. Evaluation of [^{11}C]laniquidar as a tracer of P-glycoprotein: radiosynthesis and biodistribution in rats. Nucl. Med. Biol. 2009; 36(6):643–649. [PubMed: 19647170]
14. van Waarde A, Ramakrishnan NK, Rybczynska AA, Elsinga PH, Berardi F, de Jong JR, Kwizera C, Perrone R, Cantore M, Sijbesma JWA, Dierckx RA, Colabufo NA. Synthesis and preclinical evaluation of novel PET probes for p-glycoprotein function and expression. J Med. Chem. 2009; 52(14):4524–4532. [PubMed: 19530699]
15. Hyafil F, Vergely C, Du Vignaud P, Grand-Perret T. In vitro and in vivo reversal of multidrug resistance by GF120918, an acridonecarboxamide derivative. Cancer Res. 1993; 53(19):4595–4602. [PubMed: 8402633]
16. Berny H, Bsiri N, Charbit JJ, Galy AM, Soyfer JC, Galy JP, Barbe J, Sharples D, Mesa Valle CM, Mascaro C, et al. 1,4-Dimethoxy-9(10H)-acridinone derivatives. Synthesis, DNA binding studies and trypanocidal activity. Arzneimittelforschung. 1992; 42(5):674–679. [PubMed: 1530683]
17. Sharp MJ, Mader CJ, Strachan C. Synthesis of acridine derivate multidrug-resistant inhibitors. PCT Int. Appl. WO 98/52923 A1. 1998
18. Bobbitt JM, Sih JC. Synthesis of isoquinolines. VII. 4-Hydroxy-1,2,3,4-tetrahydroisoquinolines. J. Org. Chem. 1968; 33(2):856–858.
19. Bobbitt JM, Winter DP, Kiely JM. Synthesis of Isoquinolines. IV.1 4-Benzylisoquinolines. J. Org. Chem. 1965; 30(7):2459–2460.

20. Cutler L, Howes C, Deeks NJ, Buck TL, Jeffrey P. Development of a P-glycoprotein knockout model in rodents to define species differences in its functional effect at the blood-brain barrier. J. Pharm. Sci. 2006; 95(9):1944–1953. [PubMed: 16850390]
21. de Vries NA, Zhao J, Kroon E, Buckle T, Beijnen JH, van Tellingen O. P-glycoprotein and breast cancer resistance protein: two dominant transporters working together in limiting the brain penetration of topotecan. Clin. Cancer Res. 2007; 13(21):6440–6449. [PubMed: 17975156]
22. Wallstab A, Koester M, Bohme M, Keppler D. Selective inhibition of MDR1 P-glycoprotein-mediated transport by the acridone carboxamide derivative GG918. Br. J. Cancer. 1999; 79(7-8): 1053–1060. [PubMed: 10098736]
23. Martin C, Berridge G, Higgins CF, Mistry P, Charlton P, Callaghan R. Communication between multiple drug binding sites on P-glycoprotein. Mol. Pharmacol. 2000; 58(3):624–632. [PubMed: 10953057]
24. Polli JW, Wring SA, Humphreys JE, Huang L, Morgan JB, Webster LO, Serabjit-Singh CS. Rational use of in vitro P-glycoprotein assays in drug discovery. J. Pharmacol. Exp. Ther. 2001; 299(2):620–628. [PubMed: 11602674]
25. de Bruin M, Miyake K, Litman T, Robey R, Bates SE. Reversal of resistance by GF120918 in cell lines expressing the ABC half-transporter, MXR. Cancer Lett. 1999; 146(2):117–126. [PubMed: 10656616]
26. Kuppens IE, Witteveen EO, Jewell RC, Radema SA, Paul EM, Mangum SG, Beijnen JH, Voest EE, Schellens JH. A phase I, randomized, open-label, parallel-cohort, dose-finding study of elacridar (GF120918) and oral topotecan in cancer patients. Clin. Cancer Res. 2007; 13(11):3276–3285. [PubMed: 17545533]
27. Colabufo NA, Berardi F, Cantore M, Perrone MG, Contino M, Inglese C, Niso M, Perrone R, Azzariti A, Simone GM, Porcelli L, Paradiso A. Small P-gp modulating molecules: SAR studies on tetrahydroisoquinoline derivatives. Bioorg. Med. Chem. 2008; 16:362–373. [PubMed: 17936633]
28. Syvänen S, Xie R, Sahin S, Hammarlund-Udenaes M. Pharmacokinetic consequences of active drug efflux at the blood-brain barrier. Pharm Res. 2006; 23(4):705–717. [PubMed: 16575498]
29. Langer O, Kuntner C, Bankstahl JP, Bankstahl M, Wanek T, Stanek J, Müller M, Löscher W. Mapping regional P-gp function in normal and epileptic rat brain with (R)–[11C]verapamil PET [symposium abstract]. J Nucl Med. 2009; 50(Supplement 2):158P.
30. Bergström M, Grahnen A, Langström B. Positron emission tomography microdosing: a new concept with application in tracer and early clinical drug development. Eur. J. Clin. Pharmacol. 2003; 59(5-6):357–366. [PubMed: 12937873]
31. Larsen P, Ulin J, Dahlstrøm K, Jensen M. Synthesis of [^{11}C]iodomethane by iodination of [^{11}C]methane. Appl. Radiat. Isot. 1997; 48(2):153–157.
32. Jewett DM. A simple synthesis of [^{11}C]methyl triflate. Appl. Radiat. Isot. 1992; 43:1383–1385.
33. Abrahim A, Luurtsema G, Bauer M, Karch R, Lubberink M, Pataraia E, Joukhadar C, Kletter K, Lammertsma AA, Baumgartner C, Müller M, Langer O. Peripheral metabolism of (*R*)-[(^{11})C]verapamil in epilepsy patients. Eur. J. Nucl. Med. Mol. Imaging. 2008; 35:116–123. [PubMed: 17846766]
34. Loening AM, Gambhir SS. AMIDE: a free software tool for multimodality medical image analysis. Mol. Imaging. 2003; 2(3):131–137. [PubMed: 14649056]

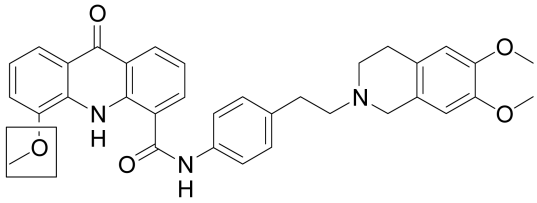

Elacridar (**1**)

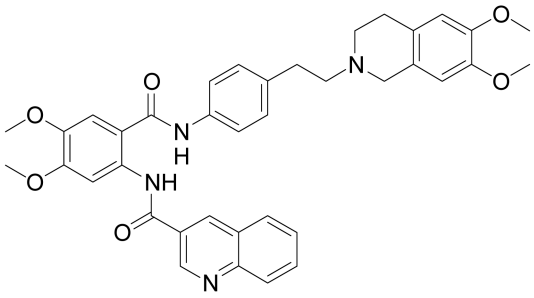

Tariquidar

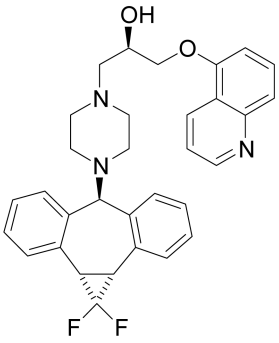

Zosuquidar

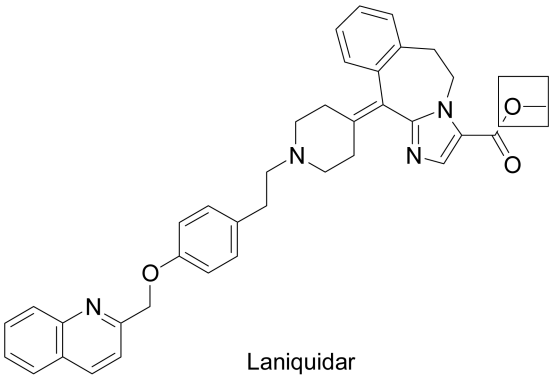

Laniquidar

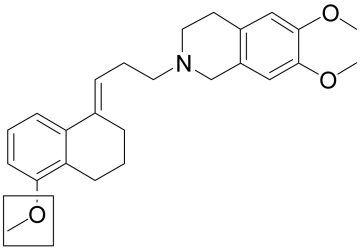

MC-18

Figure 1.
Third-generation P-gp inhibitors. For compounds used as PET tracers, the position of the ^{11}C-label is indicated by the square.

Europe PMC Funders Author Manuscripts

Europe PMC Funders Author Manuscripts

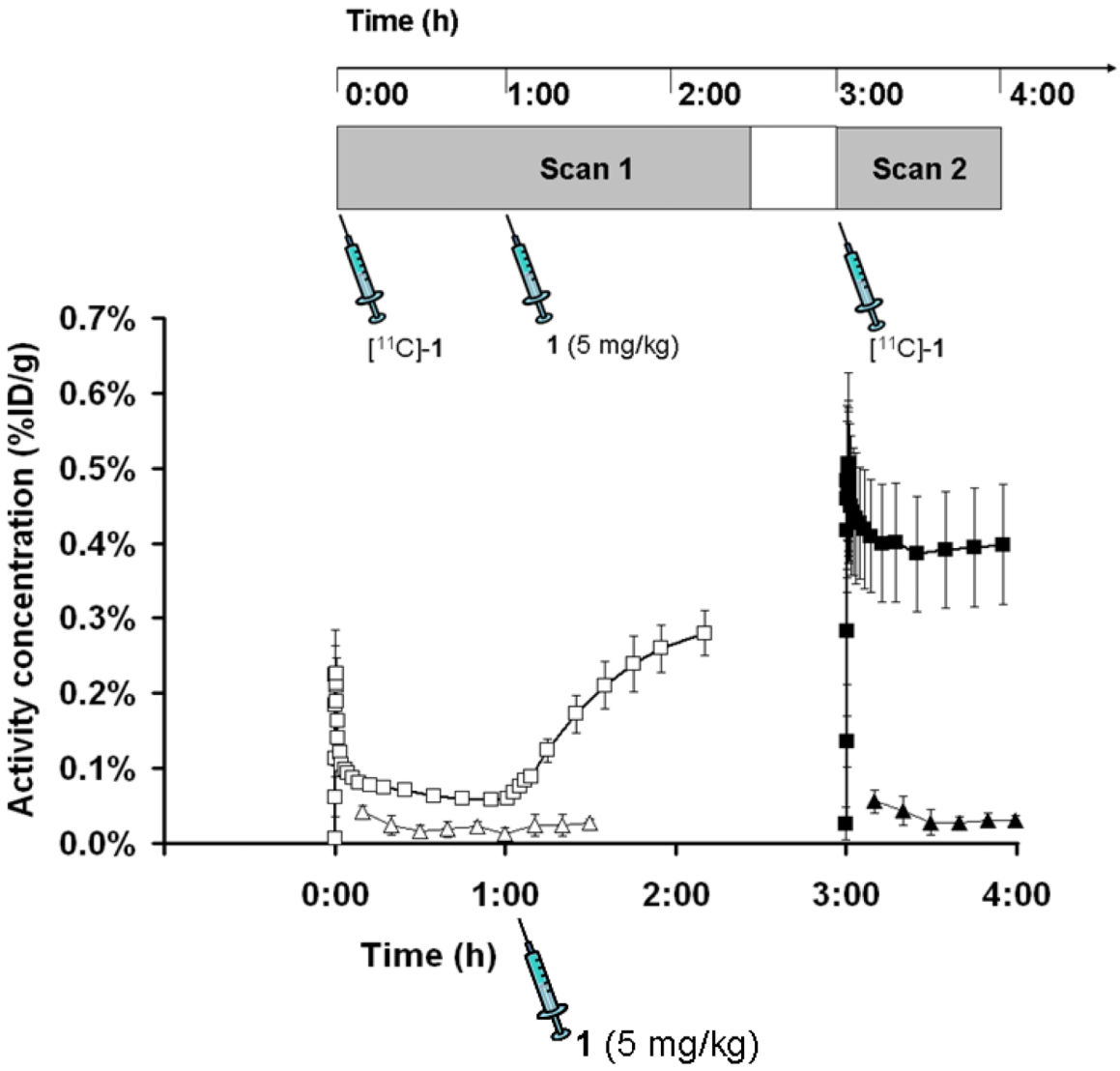

Figure 2.

TACs (mean %ID/g±SD, n=3) of [^{11}C]-**1** in whole brain (scan 1: open squares, scan 2: closed squares) and arterial blood (scan 1: open triangles, scan 2: closed triangles) for the paired PET scans in rats. Unlabeled **1** (5 mg/kg) was administered as an i.v. bolus at 60 min after start of scan 1 (see timeline above).

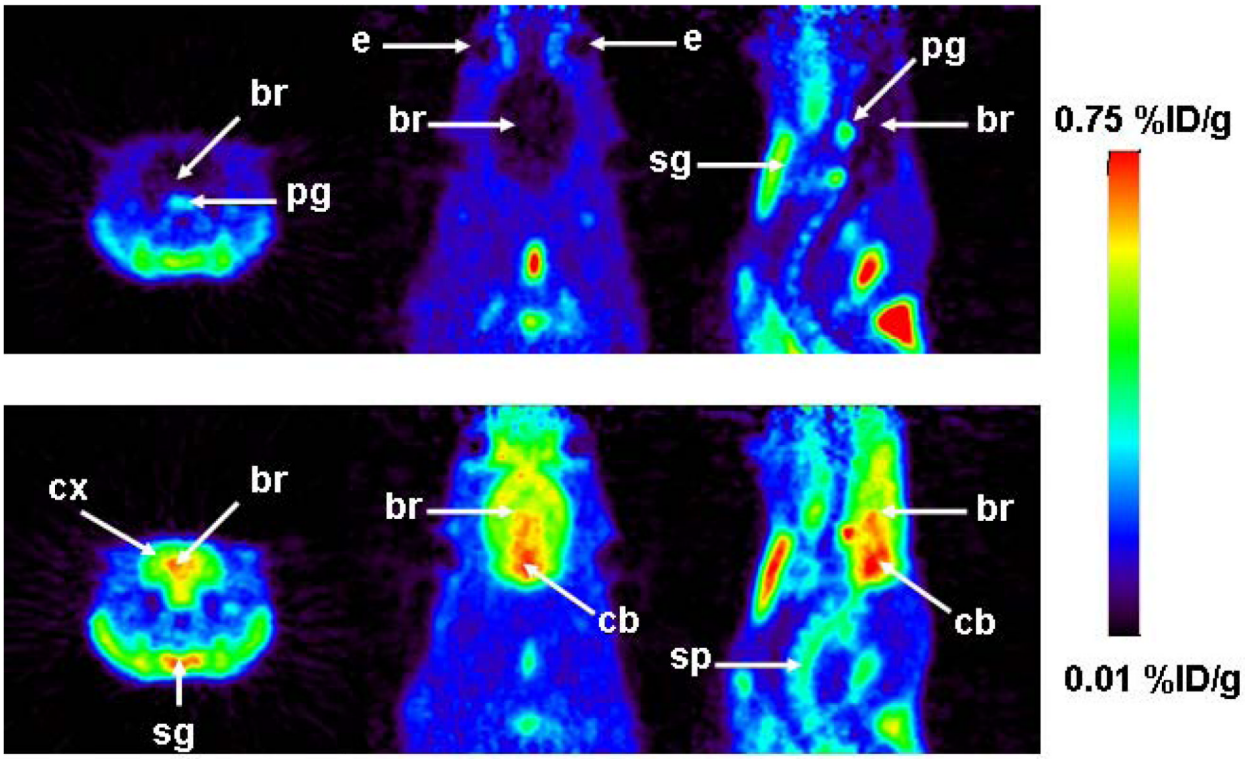

Figure 3.

Coronal (left), horizontal (center) and sagittal (right) PET summation images depicting the distribution of radioactivity following i.v. injection of [^{11}C]-**1** in a rat before (scan 1: 0-60 min, upper row) and after (scan 2: 0-60 min, lower row) administration of unlabeled **1** (5 mg/kg). Activity concentration is expressed as %ID/g. The radiation scale is set from 0.01 to 0.75 %ID/g; dark colors indicate low and bright colors indicate high activity concentrations. Anatomical structures are indicated by arrows (br, brain; cx, cortex; cb, cerebellum; e, eye; sg, submandibular gland; pg, pituitary gland; sp, spine).

Europe PMC Funders Author Manuscripts

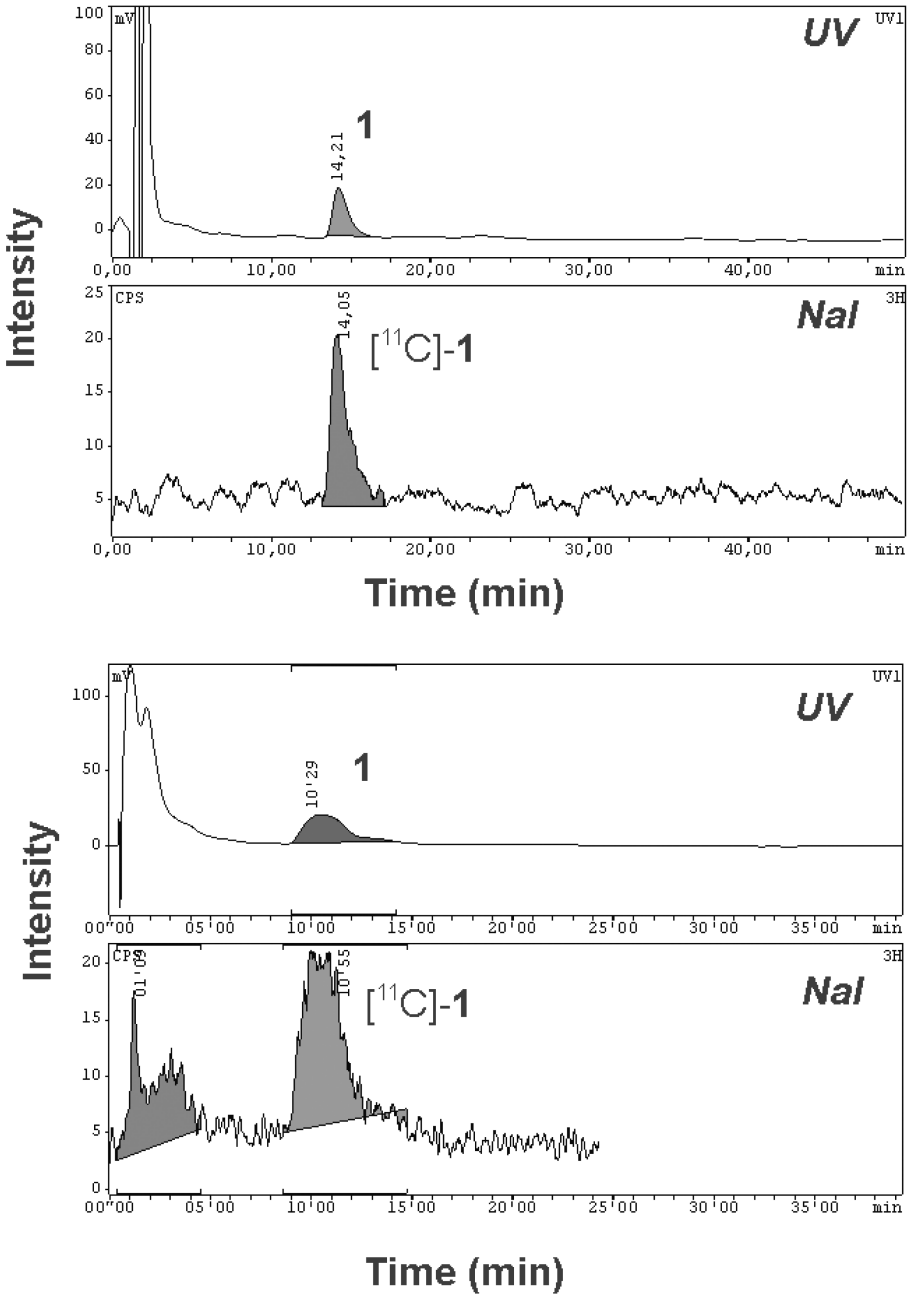

Figure 4.

Radio-HPLC chromatograms of SPE eluates of arterial plasma samples collected at 20 min (upper chromatogram) and at 60 min (lower chromatogram) after injection of [^{11}C]-**1** into rat. In the upper channel UV absorption (wavelength: 227 nm) and in the lower channel radioactivity is measured. Plasma samples were spiked with unlabeled **1**. For HPLC conditions see experimental section.

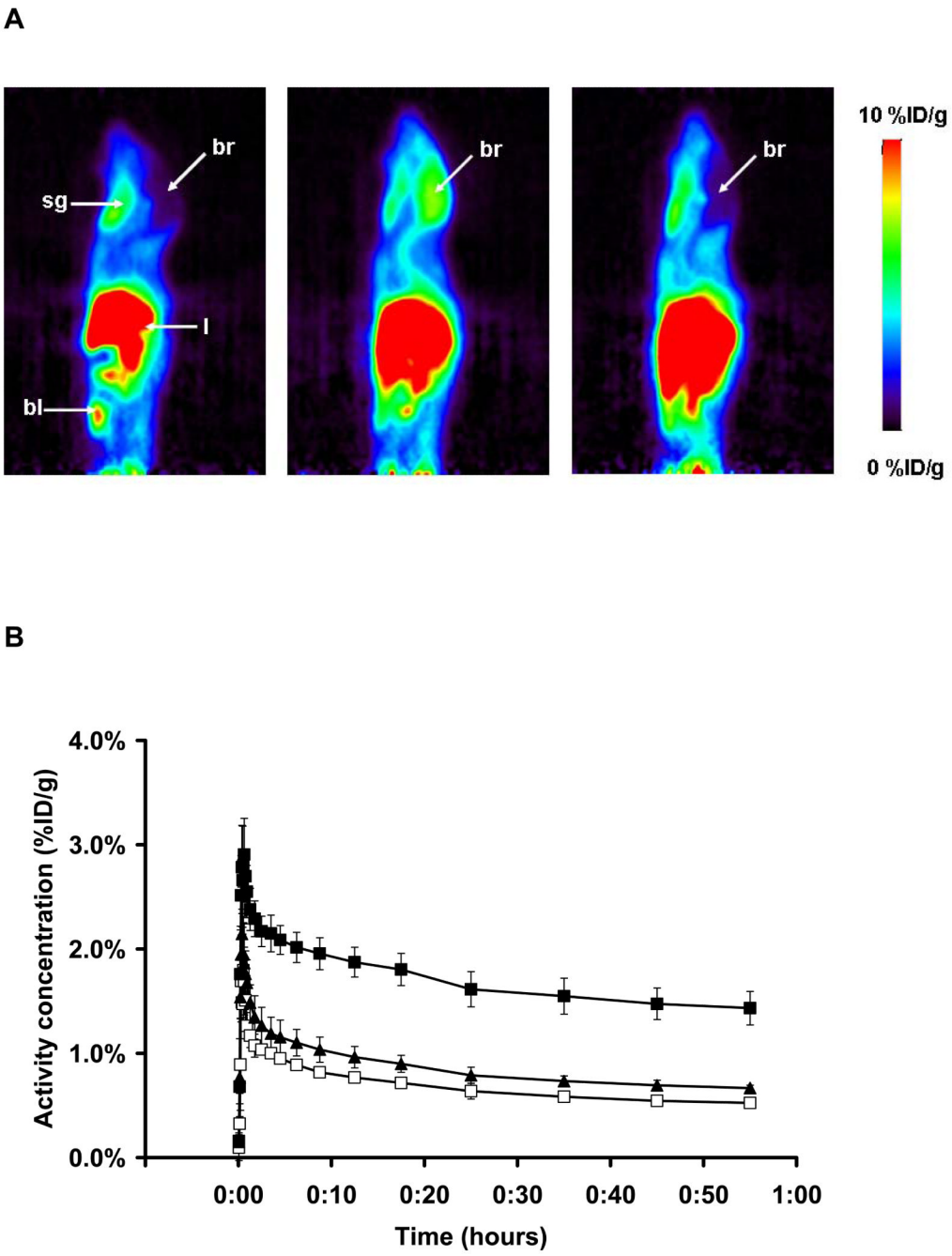

Figure 5.

A: Sagittal PET summation images (0-60 min) depicting the distribution of radioactivity following i.v. injection of [^{11}C]-**1** into a wild-type mouse (left), a *Mdr1a/b*$^{(-/-)}$ mouse (center) and a *Bcrp1*$^{(-/-)}$ mouse (right). Activity concentration is expressed as %ID/g and the radiation scale is set from 0 to 10 %ID/g. Anatomical structures are indicated by arrows (br, brain; bl, bladder; l, liver; sg, submandibular gland). **B**: TACs (mean %ID/g±SD) of [^{11}C]-**1** in whole brain of wild-type (open squares, n=3), *Mdr1a/b*$^{(-/-)}$ (closed squares, n=3) and *Bcrp1*$^{(-/-)}$ (closed triangles, n=3) mice.

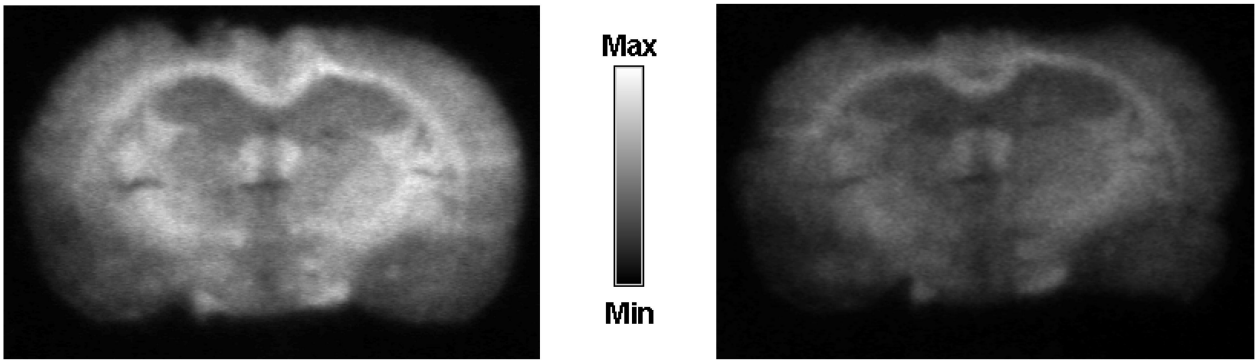

Figure 6.
In vitro autoradiography of coronal rat brain slices (10 μm) incubated with [^{11}C]-**1** alone (left) and with [^{11}C]-**1** and an excess of unlabeled **1** (1 μM, right).

Europe PMC Funders Author Manuscripts

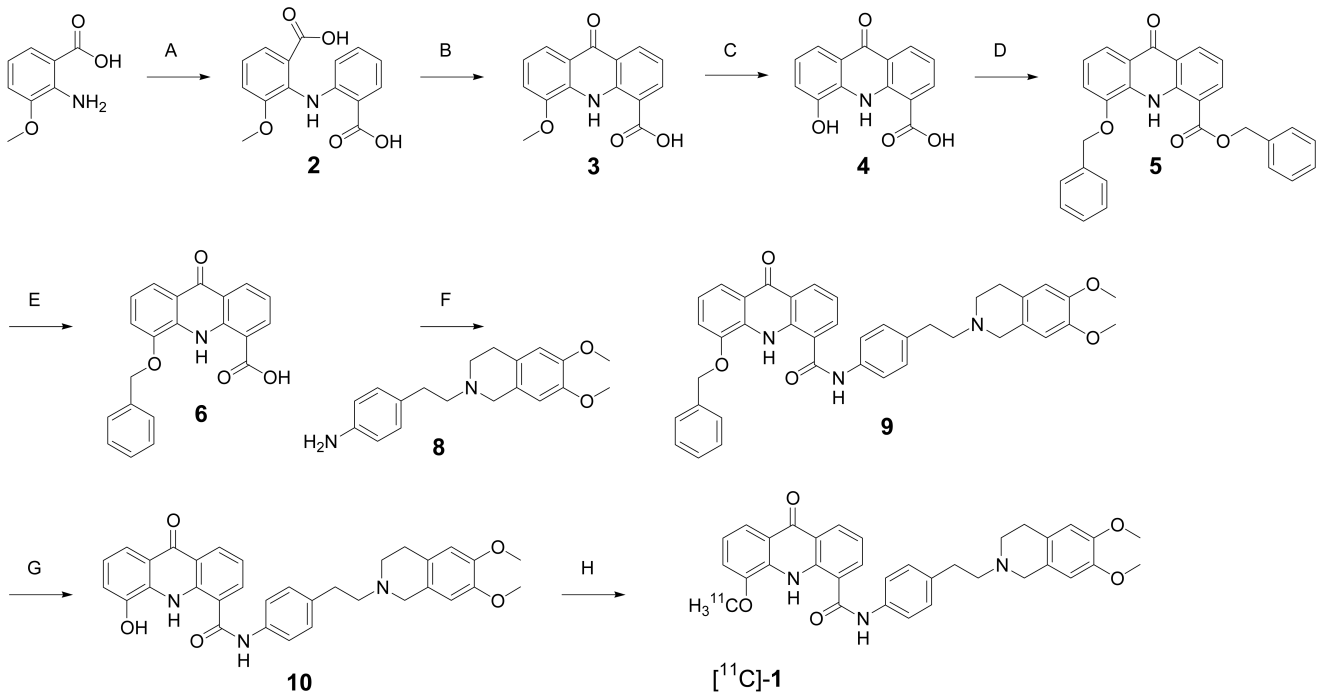

Reagents (**A**): 2-Bromobenzoic acid, Cu^0/K_2CO_3, EtOH, reflux; (**B**) $POCl_3$, CH_3CN, reflux; (**C**): HBr, Ac_2O, reflux (**D**): BnCl, K_2CO_3, DMF, 50°C; (**E**): aq. LiOH, MeOH, reflux; (**F**): TBTU, Et_3N, DMF, rt; (**G**): Pd/C, H_2, EtOH, rt; (**H**): $[^{11}C]CH_3OTf$, acetone, aq. NaOH, 60°C

Scheme 1.

Synthesis of **10** and its radiolabeling with $[^{11}C]$-methyl triflate to give $[^{11}C]$-**1**.

Europe PMC Funders Author Manuscripts